Current Journal of Applied Science and Technology

39(35): 12-27, 2020; Article no.CJAST.61707
ISSN: 2457-1024
(Past name: British Journal of Applied Science & Technology, Past ISSN: 2231-0843, NLM ID: 101664541)

Effects of Anisotropy on Natural Convection in a Vertical Porous Cavity Filled with a Heat Generation

Degan Gerard[1], Sokpoli Amavi Ernest[2*], Akowanou Djidjoho Christian[1] and Vodounnou Edmond Claude[2]

[1]Laboratory of Energetic and Applied Mechanics (LEMA), National University of Science, Technology, Engineering and Mathematics (UNSTIM), Abomey; BP 2282, Goho Abomey, Benin.
[2]Laboratory of Energetic and Applied Mechanics (LEMA), EPAC - UAC, 01 BP 526, Cotonou, Benin.

Authors' contributions

This work was carried out in collaboration among all authors. Author SAE designed the study, performed the statistical analysis, wrote the protocol and wrote the first draft of the manuscript. Authors DG and ADC managed the analyses of the study. Author VEC managed the literature searches. All authors read and approved the final manuscript.

Article Information

DOI: 10.9734/CJAST/2020/v39i3531049
Editor(s):
(1) Dr. Elena Lanchares Sancho, University of Zaragoza, Spain.
Reviewers:
(1) B. G. Sumana, Government Engineering College, Hassan, India.
(2) Mirza Humaun Kabir Rubel, University of Rajshahi, Bangladesh.
Complete Peer review History: http://www.sdiarticle4.com/review-history/61707

Original Research Article

Received 04 August 2020
Accepted 11 October 2020
Published 17 November 2020

ABSTRACT

This research was devoted to the analytical study of heat transfer by natural convection in a vertical cavity, confining a porous medium, and containing a heat source. The porous medium is hydrodynamically anisotropic in permeability whose axes of permeability tensor are obliquely oriented relative to the gravitational vector and saturated with a Newtonian fluid. The side walls are cooled to the temperature T'_c and the horizontal walls are kept adiabatic. An analytical solution to this problem is found for low Rayleigh numbers by writing the solutions of mathematical model in polynomial form of degree n of the Rayleigh number. Poisson equations obtained are solved by the modified Galerkin method. The results are presented in term of streamlines and isotherms. The distribution of the streamlines and the temperature fields are greatly influenced by the permeability anisotropy parameters and the thermal conductivity. The heat transfer decreases considerably when the Rayleigh number increases.

**Corresponding author: E-mail: ermavli@yahoo.fr;*

Keywords: *Natural convection; anisotropic porous medium; vertical rectangular cavity; Nusselt number; heat generation.*

NOMENCLATURES

a, b, c	*: Constants*
A	*: Aspect ratio of the cavity*
f_1	*: Approximate function*
$\vec{g}$	*: Vector gravity field*
H'	*: Height of the cavity*
j, n	*: Index*
$\bar{\bar{K}}'$	*: Second-order permeability tensor*
K_1, K_2	*: Flow permeability along the principal axes*
K^*	*: Permeability ratio*
$k_{x'}, k_{y'}$	*: Thermal conductivity*
k^*	*: Thermal conductivity ratio*
L'	*: Thickness of the cavity*
$L_0, L_1, \dots, L_{12}$	*: Functions*
Nu	*: Overall Nusselt number*
P'	*: Pressure of the saturating vapor*
Ra	*: Rayleigh number*
S'	*: Constant volumetric heat generation*
$T_0, T_1, T_2, \dots$	*: Temperature perturbation functions*
T'	*: Dimensional fluid temperature*
T_c'	*: Dimensional temperature at left vertical wall*
T_h'	*: Dimensional temperature at right vertical wall*
T	*: Dimensionless fluid temperature*
$\Delta T' = (T_h' - T_c')$	*: Temperature difference scale*
u', v'	*: Dimensional velocities in x and y directions*
u, v	*: Dimensionless velocities in x and y directions*
$\vec{V}'$	*: Vector velocity of filtration of the fluid in porous medium*
x'	*: Dimensional Cartesian coordinate measured along the vertical wall of the cavity*
y'	*: Dimensional Cartesian coordinate measured along the bottom wall of the cavity*
x, y	*: Dimensionless Cartesian coordinates*
$\bar{\bar{\alpha}}'$	*: Thermal diffusivity tensor*
α_1, α_2	*: Functions*
β	*: Coefficient of thermal expansion of fluid*
μ	*: Dynamic viscosity of the fluid*
ν	*: Kinematic viscosity of the fluid*
$\zeta, \xi, \varsigma, \omega$	*: Characteristic roots, functions*
ϱ	*: Density of the fluid*
ϕ_1	*: Approximate function*
$(\varrho C_p)_f$	*: Heat capacity of the fluid*
ψ	*: Dimensionless stream function*
$\psi_0, \psi_1, \psi_2, \dots$	*: Perturbation stream function*

1. INTRODUCTION

The heat transfer through natural convection induced by an internal heat source, in a vertical cavity filled with granular porous medium finds many applications in engineering. In order not to limit the field, we may be mentioned the heat extraction debris of nuclear fuel in nuclear reactors as well as the underground storage of radioactive waste. The same phenomenon is observed when examining of porous underground layers when we can expect a radioactive heating, either naturally or because of the proximity of nuclear waste.

The natural convection generated by an internal heat source is observed during drying and storage of granular agricultural products at sunset. So the agricultural products stored in the dryer are generated by metabolism. Due to the temperature difference between the interior of the cavity and the side walls, there is a natural convection where the air flow is directed downwardly in the vicinity of the vertical walls and upward in the central portion of the cavity .This exchange induced by internal heat source has been the subject of several researches in the past. Meffert and Potters [1], on the first hand and Rooda Eckman and Van Beckum [2] on the other hand, carried out calculations on cooling rates and temperature distributions in closed containers for the design of cold storage facilities. In the research, natural convection is neglected. The authors Hwang [3]; Buretta [4]; Sun [5]; Gabor et al. [6]; Gasser and Kazimi [7]; Hardee and Nilson [8] have also investigated on the effects of heat from internal sources in porous media.

Bergholz [9] considered the convective flow in the boundary layer regime in a closed rectangular enclosure. The fluid constituting the heat source of internal heat is cooled by the side walls of the cavity. The author employed a computational procedure, based on the technique developed by Gill [10] which modified the Oseen linearization method to solve the system of equations valid for the boundary layer region. He discovered a bicellular circulation of the convective flux which occurs by its descent at the side walls in the boundary layer region and ascent in the central region. This increase generates a strong and stable vertical temperature gradient in the central region of the cavity. The distribution of heat flow over the side walls indicates that most of the internal heat is vented along the top half of the side wall. Natural convection with a uniform volumetric energy source in a confined fluid with insulated side and bottom walls and rigid top wall or free top surface, was analyzed numerically by Emara and Kulacki [11]. This authors obtained temperature profiles and Nusselt number within the fluid that were in good agreement with experiment data. Beukema et al. [12] continued the research for the storage of agricultural products, in developing a three-dimensional model to study the natural convection in a confined porous medium and filled with a heat source.

Later, a theoretical study on the natural convection in a rectangular enclosure containing a uniform heat source and cooled by the side walls was realized by Haajizadeh et al. [13]. They obtained asymptotic solutions for low and high Rayleigh numbers. For low Rayleigh numbers, they solved the problem by using the modified Galerkin method to solve the obtained Poisson's equations. Considering the high numbers of Rayleigh, they examined the boundary layer equations as well in the central region of the enclosure as close to sidewalls. A two-dimensional numerical study of natural convection of air in a vertical or inclined square box was conducted by Acharva and Goldstein [14]. The cavity is heated from the outside and contains a uniformly distributed heat source. Prasad [15] conducted a numerical study of the permanent two-dimensional flow in a rectangular cavity filled with a porous medium and containing a heat source. The side walls are maintained isothermal and horizontal ones are adiabatic. The temperature at any place in the cavity increases with the Rayleigh number (Ra) and the rate of increase decreases with an increase in Ra and the aspect ratio A. The maximum temperature in the cavity increases constantly with A and Ra while the rate of increase decreases with this increase in A and Ra. The local Nusselt number on the side walls is a function of A, Ra and the boundary conditions. The heat transfer rates are close to those of the heated cavity by applying a uniform heat flow. Churbanov et al. [16] analyzed numerically by the finite difference method, the natural convection in a rectangular enclosure. The enclosure walls are isothermal or adiabatic and the fluid is a heat source. They made a comparison of the solutions obtained relating to experimental and numeric data obtained in the past.

Recently, Kim and Hyun [17] studied numerically, convection induced by the buoyancy force, in a rectangular enclosure filled with a porous medium, heat, and saturated with a non-Newtonian fluid. The side walls are cooled and the horizontal ones are adiabatic. The flow of non-Newtonian fluid through the porous medium is described by Darcy's equation. For a Rayleigh number and a given aspect ratio, compared to a Newtonian fluid, convective activity is more intense for $n < 1$ and less intense for $n > 1$. An increase of the aspect ratio weakens the convection. In addition, for an increase in the aspect ratio or the flow index n, the thermal flow changes to the boundary layer regime.

This study describes the natural convection in a vertical porous cavity filled with a uniform heat

source and cooled side walls. The porous medium is supposed to be anisotropy in permeability and the main directions of permeability make an arbitrary angle with the vertical. An asymptotic solution is determined for low Rayleigh numbers. We examined the influence of the anisotropy in permeability and conductivity on the heat transfer.

2. MATERIALS AND METHODS

2.1 Description of the Physical Model

We consider a two-dimensional vertical rectangular enclosure filled with a porous medium characterized by an anisotropic permeability with a constant volumetric heat generation S', as shown in Fig. 1. The granular cereal products contained in the cavity represent the porous medium and the internal heat source is the combined result of the metabolism of the cereal products as well as the heat accumulated during the day.

L' and H' are the width and the height, respectively, of the vertical rectangular enclosure with an aspect $A = 2$. The horizontal walls are insulated and the vertical walls are at uniform temperature T_c'. The permeabilities along the two principal axes of the porous medium are denotes by K_1 and K_2. The anisotropy of the porous medium is then represented by the anisotropy ratio $K^* = K_1/K_2$ and the orientation angle φ, defined as the angle between the horizontal direction and the principal axis with permeability K_2.

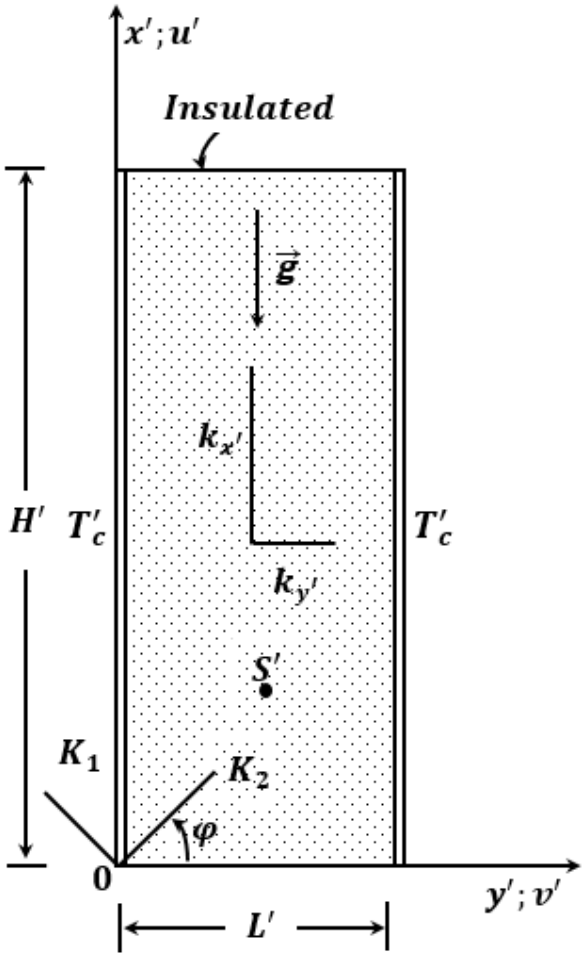

Fig. 1. Physical situation and coordinates system

2.2 Governing Equations

The vertical rectangular enclosure boundary is assumed to be impermeable to the saturating fluid (air). The saturating fluid is incompressible, and its motion through the porous medium obeys Darcy's law. The fluid and the porous medium are assumed to be in thermal equilibrium and the thermo-physical properties of the fluid are assumed constant, except for the density in the buoyancy term in the momentum equation (Degan and Vasseur [18]).

Under these assumptions, the conservation equations for momentum and energy transfer can be written as (Bear [19]):

$$\nabla \vec{V}' = 0 \tag{1}$$

$$\vec{V}' = \frac{\bar{\bar{K}}'}{\mu}(-\nabla P' + \varrho \vec{g}) \tag{2}$$

$$\nabla \cdot \left(\vec{V}' T' - \bar{\bar{\alpha}}' \nabla T'\right) = \frac{S'}{\left(\varrho C_p\right)_f} \tag{3}$$

In these equations, $\vec{\boldsymbol{V}}', (\boldsymbol{u}', \boldsymbol{v}'), \bar{\bar{\boldsymbol{K}}}', \boldsymbol{\mu}, \boldsymbol{P}', \boldsymbol{\varrho}, \vec{\boldsymbol{g}}, \boldsymbol{T}', \boldsymbol{C_p}, \boldsymbol{S}'$ and $\bar{\bar{\boldsymbol{\alpha}}}'$ indicate Darcy-velocity vector, $\boldsymbol{x}'$ and $\boldsymbol{y}'$ component of Darcy velocity, permeability tensor of porous medium, dynamic viscosity, pressure, fluid density, gravitational acceleration, temperature, specific heat, constant volumetric heat generation and thermal conductivity tensor of the saturated porous medium, respectively. The second-order permeability tensor $\bar{\bar{\boldsymbol{K}}}'$ and thermal conductivity tensor $\bar{\bar{\boldsymbol{\alpha}}}'$ are defined as:

$$\bar{\bar{K}}' = \begin{bmatrix} K_1 cos^2\varphi + K_2 sin^2\varphi & (K_1 - K_2) sin\varphi cos\varphi \\ (K_1 - K_2) sin\varphi cos\varphi & K_1 sin^2\varphi + K_2 cos^2\varphi \end{bmatrix} \tag{4}$$

$$\bar{\bar{\alpha}}' = \begin{bmatrix} \alpha_{x'} & 0 \\ 0 & \alpha_{y'} \end{bmatrix} \tag{5}$$

Introducing the Boussinesq approximation,

$$\varrho = \varrho_0[1 - \beta(T' - T_c')] \tag{6}$$

eliminating the pressure term in the momentum equation in the usual way, and taking $\boldsymbol{L}', \boldsymbol{\alpha_{y'}}/\boldsymbol{L}'$ and $\boldsymbol{k_{y'}}/\boldsymbol{S}'\boldsymbol{L}'$ as respective dimensional scales for length, velocity, and temperature, the governing equations may be written in non-dimensional form as:

$$a\frac{\partial^2\psi}{\partial y^2} - 2c\frac{\partial^2\psi}{\partial x \partial y} + b\frac{\partial^2\psi}{\partial x^2} = -Ra\frac{\partial T}{\partial y} \tag{7}$$

$$u\frac{\partial T}{\partial y} + v\frac{\partial T}{\partial y} = k^*\frac{\partial^2 T}{\partial x^2} + \frac{\partial^2 T}{\partial y^2} + 1 \tag{8}$$

where $\boldsymbol{k}^*$ is anisotropy of fluid thermal conductivity and $\boldsymbol{\psi}$ is a dimensionless stream function defined as:

$$u = -\frac{\partial \psi}{\partial y}, v = \frac{\partial \psi}{\partial x} \tag{9}$$

such that equation (1) is identically satisfied.

$$\left.\begin{aligned} a &= cos^2\varphi + K^* sin^2\varphi \\ b &= sin^2\varphi + K^* cos^2\varphi \\ c &= (1 - K^*) sin\varphi cos\varphi \\ K^* &= K_1/K_2\,, k^* = k_{x'}/k_{y'} \end{aligned}\right\} \tag{10}$$

The Rayleigh number is defined as:

$$Ra = \frac{K_1 \beta g S' L'^3}{\alpha_{y'} \nu k_{y'}} \tag{11}$$

The corresponding boundary conditions can be written as:

$$\psi = 0;\ \frac{\partial T}{\partial x} = 0 \text{ at } x = 0, A \tag{12}$$

$$\psi = 0;\ T = 0 \text{ at } y = 0{,}1 \tag{13}$$

Where $\boldsymbol{A} = \boldsymbol{H}'/\boldsymbol{L}'$ is the cavity aspect ratio.

The dimensionless heat transfer across the enclosure filled with a porous medium is characterized by the Nusselt number defined as [11]:

$$Nu = \frac{2}{A}\int_0^A \left(\frac{\partial T}{\partial y}\right)_{y=0} dx \tag{14}$$

Owing to the symmetry of the problem, the vertical center line is a stagnation streamline dividing the flow into two cells which are mirror images of each other. Consequently the present results can be employed as well for a 2-D porous enclosure cooled at only one vertical wall with other walls insulated [13].

3. SOLUTION BY PERTURBATION METHOD

Let us consider now a solution by the regular perturbation method for this problem by

expanding the dependent variables $\boldsymbol{\psi}$ and $\boldsymbol{T}$, in the power series of $\boldsymbol{Ra}$. An approximate analytical solution is presented for the case of convection at small Rayleigh number.

$$\psi = \sum_{n=0}^{\infty} Ra^n \psi_n(x,y) \tag{15}$$

$$T = \sum_{n=0}^{\infty} Ra^n T_n(x,y) \tag{16}$$

The zeroth order solution for $\boldsymbol{\psi_0}$ and $\boldsymbol{T_0}$ are obtained from the following Poisson equations.

$$\left(a\frac{\partial^2}{\partial y^2} - 2c\frac{\partial^2}{\partial x \partial y} + b\frac{\partial^2}{\partial x^2}\right)\psi_0 = 0 \tag{17}$$

$$\left(k^*\frac{\partial^2}{\partial x^2} + \frac{\partial^2}{\partial y^2}\right)T_0 = -1 \tag{18}$$

It can be easily shown that

$$\psi_0 = 0, T_0 = (-y^2 + y)/2 \tag{19}$$

Substitution of equations (15) and (16) into equations (7) and (8) and collection of the terms of equal power of $\boldsymbol{Ra}$, linear systems for the successive $\boldsymbol{\psi_n}$ and $\boldsymbol{T_n}$ may be obtained for $\boldsymbol{n \geq 1}$:

$$\left(a\frac{\partial^2}{\partial y^2} - 2c\frac{\partial^2}{\partial x \partial y} + b\frac{\partial^2}{\partial x^2}\right)\psi_n = -\frac{\partial T_{n-1}}{\partial y} \tag{20}$$

$$\left(k^*\frac{\partial^2}{\partial x^2} + \frac{\partial^2}{\partial y^2}\right)T_n = \sum_{j=0}^{n}\left(\frac{\partial \psi_j}{\partial x}\cdot\frac{\partial}{\partial y} - \frac{\partial \psi_j}{\partial y}\cdot\frac{\partial}{\partial x}\right)T_{n-j} \tag{21}$$

By using the modified Galerkin method (Kantorovich and Krylov [20]), the above series of Poisson equations are sequentially reduced to ordinary differential equations.

The first order correction for $\boldsymbol{\psi_1}$ and $\boldsymbol{T_1}$ are obtained by the following Poisson equations.

$$\left(a\frac{\partial^2}{\partial y^2} - 2c\frac{\partial^2}{\partial x \partial y} + b\frac{\partial^2}{\partial x^2}\right)\psi_1 = -\frac{\partial T_0}{\partial y} \tag{22}$$

$$\left(k^*\frac{\partial^2}{\partial x^2} + \frac{\partial^2}{\partial y^2}\right)T_1 = \frac{\partial \psi_1}{\partial x}\cdot\frac{\partial T_0}{\partial y} \tag{23}$$

An approximate solution for $\boldsymbol{\psi_1}$ can be found in the form

$$\psi_1(x,y) = f_1(x)\phi_1(y) \tag{24}$$

where $\boldsymbol{\phi_1(y)}$ is a function chosen a priori which satisfies boundary conditions

$$\phi_1(y) = 0 \text{ on } x = 0,1 \tag{25}$$

Substituting equation (24) into equation (22), we have

$$a\frac{d^2\phi_1}{dy^2} = -\frac{dT_0}{dy} \tag{26}$$

$\boldsymbol{\phi_1(y)}$ may be obtained by integrating equation (26) as equation (27)

$$\phi_1(y) = (2y^3 - 3y^2 + y)/12a \tag{27}$$

Introducing equation (24) in the variational equation corresponding to the Poisson equation yields, the equation (28) can be obtained

$$\int_0^1 \left[\left(a\frac{\partial^2}{\partial y^2} - 2c\frac{\partial^2}{\partial x \partial y} + b\frac{\partial^2}{\partial x^2}\right)\psi_1(x,y) + \frac{\partial T_0(x,y)}{\partial y}\right]\phi_1(y)dy = 0 \tag{28}$$

The equation (28) can be transformed into the following set of ordinary differential equation for $\boldsymbol{f_1(x)}$:

$$f_1^{"} - \zeta^2 f_1 = \zeta^2 \tag{29}$$

where prime denotes differentiation with respect to $\boldsymbol{x}$.

After using the boundary conditions at $\boldsymbol{x = 0, A}$, the approximate solution for $\boldsymbol{\psi_1}$ can be obtained as:

$$\psi_1(x,y) = [sinh[\zeta(x-A)] - sinh(\zeta x) + sinh(\zeta A)](2y^3 - 3y^2 + y)/12a sinh(\zeta A) \tag{30}$$

The solution for $\boldsymbol{T_1}$ can be found by the similar method as:

$$T_1(x,y) = L_0\left\{\frac{\zeta}{sinh(\xi A)}[cosh[\xi(x-A)] - cosh(\xi x)] - \frac{\xi}{sinh(\zeta A)}[cosh[\zeta(x-A)] - cosh(\zeta x)]\right\} \times (-8y^6 + 24y^5 - 25y^4 + 10y^3 - y)/1440a \tag{31}$$

The second-order solution of $\boldsymbol{\psi_2}$ and $\boldsymbol{T_2}$ are found by solving the following Poisson equations:

$$\left(a\frac{\partial^2}{\partial y^2} - 2c\frac{\partial^2}{\partial x \partial y} + b\frac{\partial^2}{\partial x^2}\right)\psi_2 = -\frac{\partial T_1}{\partial y} \tag{32}$$

$$\left(k^*\frac{\partial^2}{\partial x^2}+\frac{\partial^2}{\partial y^2}\right)T_2=\frac{\partial\psi_1}{\partial x}\cdot\frac{\partial T_1}{\partial y}-\frac{\partial\psi_1}{\partial y}\cdot\frac{\partial T_1}{\partial x}+\frac{\partial\psi_2}{\partial x}\cdot\frac{\partial T_0}{\partial y} \tag{33}$$

The solution for equations (32) and (33) are given by:

$$\begin{aligned}\psi_2(x,y)=\Bigg[\left(L_1\frac{cosh(\xi A)-1}{sinh(\xi A)}+L_2\frac{cosh(\zeta A)-1}{sinh(\zeta A)}\right)\times\frac{sinh[\varsigma(x-A)]+sinh(\varsigma x)}{sinh(\varsigma A)}\\ +\ L_1\frac{cosh[\xi(x-A)]-cosh(\xi x)}{sinh(\xi A)}+L_2\frac{cosh[\zeta(x-A)]-cosh(\zeta x)}{sinh(\zeta A)}\Bigg]\\ \times(-16y^7+56y^6-70y^5+35y^4-7y^2+2y)/20160a^2\end{aligned} \tag{34}$$

$$\begin{aligned}T_2=\Bigg\{\Bigg[L_3\frac{cosh(\zeta A)-1}{sinh(\zeta A)}+L_4\frac{cosh(\xi A)-1}{sinh(\xi A)}\Bigg]\times\frac{cosh[\varsigma(x-A)]-cosh(\varsigma x)}{sinh(\varsigma A)}\\ +L_5\frac{sinh[\zeta(x-A)]-sinh(\zeta x)}{sinh(\zeta A)}+L_6\frac{sinh[\xi(x-A)]-sinh(\xi x)}{sinh(\xi A)}\\ +L_7\left[\frac{sinh[\zeta(x-A)]-sinh(\zeta x)}{sinh(\zeta A)}\right]\times\left[\frac{sinh[\xi(x-A)]-sinh(\xi x)}{sinh(\xi A)}\right]\\ +L_8\left[\frac{cosh[\zeta(x-A)]-cosh(\zeta x)}{cosh(\zeta A)}\right]\times\left[\frac{cosh[\xi(x-A)]-cosh(\xi x)}{cosh(\xi A)}\right]\\ +L_9\left[\frac{sinh[\zeta(x-A)]-sinh(\zeta x)}{sinh(\zeta A)}\right]^2+L_{10}\left[\frac{cosh[\zeta(x-A)]-cosh(\zeta x)}{cosh(\zeta A)}\right]^2\\ +\left[L_{11}\frac{cosh(\zeta A)-1}{sinh(\zeta A)}+L_{12}\frac{cosh(\xi A)-1}{sinh(\xi A)}\right]\times\left[\frac{sinh[\omega(x-A)]+sinh(\omega x)}{sinh(\omega A)}\right]\Bigg\}\\ \times(448y^{10}-2240y^9+4410y^8-4200y^7+1470y^6+882y^5\\ -1155y^4+420y^3-35y)/50803200a^2\end{aligned} \tag{35}$$

In the above equations $\boldsymbol{\zeta, \xi, \varsigma}$ and $\boldsymbol{\omega}$ are the characteristic roots of the ordinary differential equations corresponding to $\boldsymbol{\psi_1, T_1, \psi_2}$ and $\boldsymbol{T_2}$ respectively, and the functions $\boldsymbol{L_0, L_1, \dots, L_{12}}$ are dependent of the characteristic roots. The expressions of these characteristic roots and the functions are defined as the following:

$$\left.\begin{aligned}\zeta=\sqrt{42\frac{a}{b}};\ \xi=\sqrt{\frac{4758}{421k^*}}\\ \varsigma=\sqrt{\frac{7460}{157}\frac{a}{b}}\ ;\ \omega=\sqrt{\frac{2380314}{205087k^*}}\\ \alpha_1=\frac{2188074}{205087k^*}\ ;\ \alpha_2=\frac{63084}{3061k^*}\\ L_0=\frac{\zeta\xi}{k^*(\zeta^2-\xi^2)}\ ;\ L_1=\frac{L_0\zeta\varsigma^2}{a(\xi^2-\varsigma^2)}\\ L_2=-\frac{L_0\xi\varsigma^2}{a(\zeta^2-\varsigma^2)}\ ;\ L_3=-\frac{L_2\varsigma\omega^2}{\varsigma^2-\omega^2}\\ L_4=-\frac{L_1\varsigma\omega^2}{\varsigma^2-\omega^2}\ ;\ L_5=\frac{\zeta(L_0\xi\alpha_2+L_2\omega^2)}{\zeta^2-\omega^2}\\ L_6=-\frac{\xi(L_0\zeta\alpha_2+L_1\omega^2)}{\xi^2-\omega^2}\\ L_7=-\frac{L_0\zeta\xi[\alpha_2(\zeta^2+\xi^2-\omega^2)+2\alpha_1\zeta^2]}{(\zeta^2+\xi^2-\omega^2)^2-4\zeta^2\xi^2}\\ L_8=\frac{L_0\zeta^2[\alpha_1(\zeta^2+\xi^2-\omega^2)+2\alpha_2\xi^2]}{(\zeta^2+\xi^2-\omega^2)^2-4\zeta^2\xi^2}\\ L_9=\frac{L_0\zeta\xi[\alpha_2(2\zeta^2-\omega^2)+2\alpha_1\zeta^2]}{(2\zeta^2-\omega^2)^2-4\zeta^4}\\ L_{10}=-\frac{L_0\zeta\xi[\alpha_1(2\zeta^2-\omega^2)+2\alpha_2\zeta^2]}{(2\zeta^2-\omega^2)^2-4\zeta^4}\\ L_{11}=-\frac{-\varsigma L_3+\zeta(L_5-L_7-2L_9-2L_{10})-\xi L_8}{\omega}\\ L_{12}=-\frac{-\varsigma L_4+\xi(L_6+L_7)-\zeta L_8}{\omega}\end{aligned}\right\} \tag{36}$$

The important physical characteristic for this heat transfer describes the heat transfer rate across the enclosure expressed by the average Nusselt number of the cold wall. The Nusselt number can be obtained where we know the temperature field. In the dimensionless form, the Nusselt number is computed by the temperature gradient at $\boldsymbol{y = 0}$.

$$Nu = 1 + \left[\frac{2}{A}\int_0^A \left(\frac{\partial T_2}{\partial y}\right)_{y=0} dx\right] Ra^2 \qquad (37)$$

In the equation (14), the first-order term is always zero, because the integral of the temperature gradient in $\boldsymbol{y}$ direction from $\boldsymbol{y = 0}$ to $\boldsymbol{y = A}$ is identically zero.

4. RESULTS AND DISCUSSION

This section is devoted to the discussion of the influence of conductivity anisotropy ratio $\boldsymbol{k^*}$, the direction and the relative importance of maximum and minimum permeabilities. The different effects of anisotropy in permeability and thermal conductivity on perturbation functions $\boldsymbol{\psi_1, T_1, \psi_2}$ and $\boldsymbol{T_2}$ are shown in Figs. 2 to 10, for a vertical shape ratio cavity $\boldsymbol{A = 2}$. The perturbation functions are regularly spaced and are symmetrical relative to the mid-height of the cavity.

Changes in perturbation functions $\boldsymbol{\psi_1, T_1, \psi_2}$ and $\boldsymbol{T_2}$ when the permeability anisotropy ratio ranging from **0.01** to **100** for conductivity anisotropy ratio $\boldsymbol{k^* = 1}$ and the orientation angle $\boldsymbol{\varphi = 30°}$ are illustrated in Figs. 2 to 4. In these three figures, the distortion is more remarkable at the perturbation function $\boldsymbol{\psi_2}$. Fig. 2 shows the streamlines and isotherms for a porous isotropic medium. These curve are similar to those obtained by Haajizadeh et al. [13]. In Fig. 2(a), the flow is bicellular and symmetrical along the mid-height. This behavior is due to the conduction temperature profile $\boldsymbol{T_0}$. In the upper part of the cavity, the fluid is hot enough and cannot dissipate the heat. The fluid temperature is then in this area greater than that of pure conduction. In the lower part of the cavity, the movement of the cold fluid to the bottom of the cavity, removes heat and its temperature is lower than the pure conduction temperature.

The first order temperature $\boldsymbol{T_1}$ shown in Fig. 2(b) is anti-symmetric compared to the mid-height. It is positive in the upper half and negative in the lower half of the cavity. Fig. 2(c) shows four identical cells which are symmetrical relative to the center of the cavity. In the upper half of the cavity, the second order function $\boldsymbol{\psi_2}$ improves the flow and weakens it in the lower half.

Figs. 3 and 4 show first-order isotherms which are asymmetrical with respect to the mid-height of the cavity. The isotherms are close to the half-height for $\boldsymbol{K_2 > K_1}$ and distant from the half height otherwise. The second order isotherms have three superposed cells.

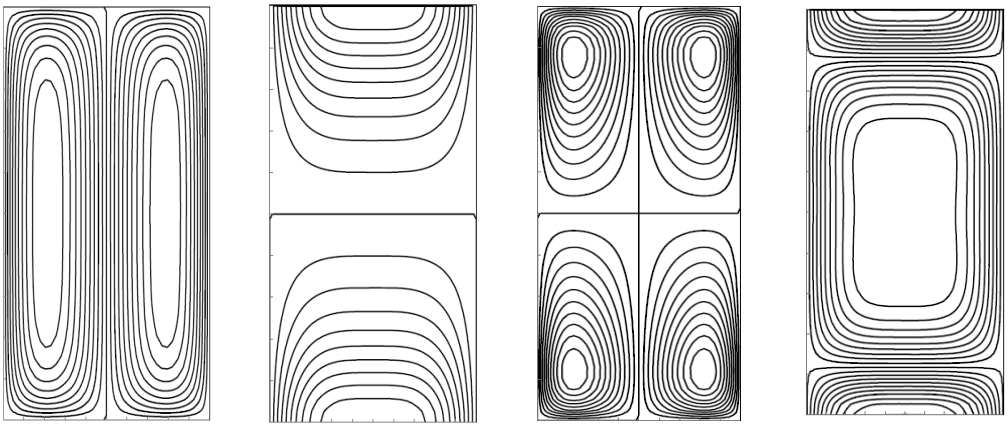

a **b** **c** **d**

Fig. 2. Streamlines and isotherms for $k^* = 1, K^* = 1$ and $\varphi = 30°$: a) $\left|\psi_{1_{max}}\right| = 8 \times 10^{-3}$; b) $T_{1_{min}} = -2.87 \times 10^{-4}$; $T_{1_{max}} = 2.87 \times 10^{-4}$; c) $\left|\psi_{2_{max}}\right| = 8.76 \times 10^{-6}$; d) $T_{2_{min}} = -3.90 \times 10^{-7}$; $T_{2_{max}} = 4.09 \times 10^{-7}$

Fig. 3 shows the isotherms and streamlines when the anisotropic permeability ratio $K^* > 1$, that is to say that the permeability in the vertical direction is smaller than the horizontal. The maximum values of, perturbation functions $\psi_1$and ψ_2 decrease. An increase in the anisotropy ratio thus delays the flow of convection flows in the cavity. In addition, Fig. 3 indicates that an increase in the anisotropic permeability ratio causes a slight detachment of the streamlines and isotherms of the vertical and horizontal walls which are concentrated in the center of the cavity. This behavior can be explained by the cooling fluid in the vertical walls of the cavity.

The opposite phenomenon is observed when the permeability in the direction of K_2 is greater than that in the direction of K_1 ($K^* < 1$) .In this situation the maxima of perturbation functions ψ_1 and ψ_2 increase, creating an important convective flow.

Fig. 4 indicates the streamlines ψ_2 which are concentrated at the four corners of the cavity while those of ψ_1 are elongated in the vertical direction and glued to the vertical walls of the cavity.

The influence of the anisotropy orientation angle φ on perturbation functions is shown in Figs. 5 to 8.

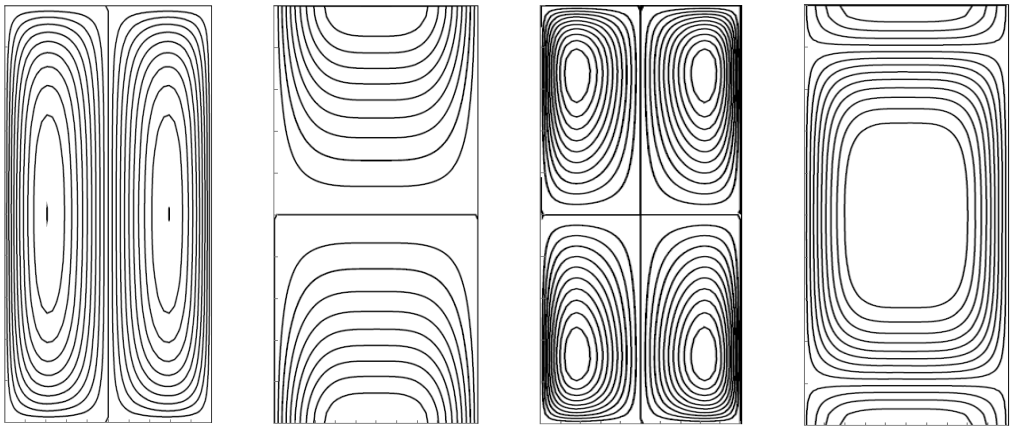

Fig. 3. Streamlines and isotherms for$k^* = 1, K^* = 100$ and $\varphi = 30°$: a) $|\psi_{1_{max}}| = 2.97 \times 10^{-4}$; b) $T_{1_{min}} = -8.89 \times 10^{-6}$; $T_{1_{max}} = 8.89 \times 10^{-6}$; c) $|\psi_{2_{max}}| = 3.19 \times 10^{-10}$; d) $T_{2_{min}} = -3.15 \times 10^{-10}$; $T_{2_{max}} = 1.13 \times 10^{-9}$

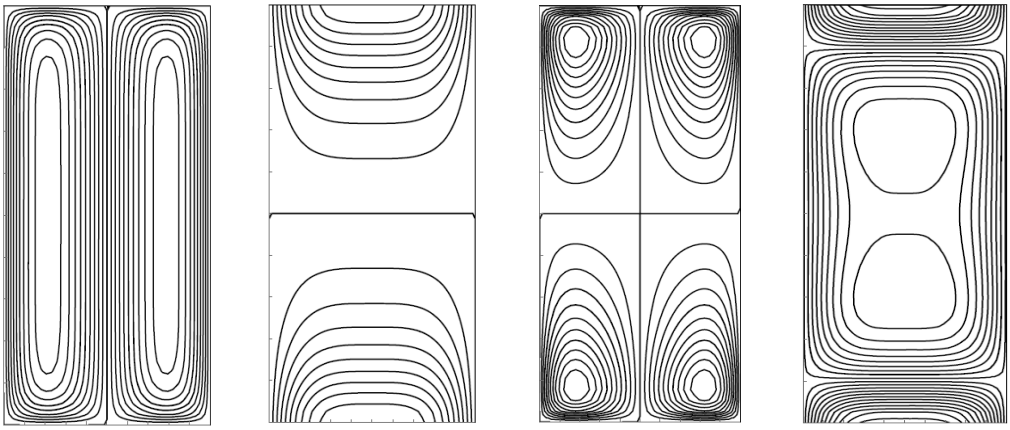

Fig. 4. Streamlines and isotherms for$k^* = 1, K^* = 0.01$ and $\varphi = 30°$: a) $|\psi_{1_{max}}| = 1.07 \times 10^{-2}$; b) $T_{1_{min}} = -4.45 \times 10^{-4}$, $T_{1_{max}} = 4.45 \times 10^{-4}$; c) $|\psi_{2_{max}}| = 2.87 \times 10^{-5}$; d) $T_{2_{min}} = -8.56 \times 10^{-7}$, $T_{2_{max}} = 9.97 \times 10^{-7}$

Among these, the Figs. 5 and 7 describe the effect of the anisotropy angle $\boldsymbol{\varphi}$ on the streamlines and isotherms $\boldsymbol{\psi_1}, \boldsymbol{T_1}, \boldsymbol{\psi_2}$ and $\boldsymbol{T_2}$ when the anisotropy ratios permeability $\boldsymbol{K^*}$ and conductivity $\boldsymbol{k^*}$ are kept constant ($\boldsymbol{K^* = 100}$ and $\boldsymbol{k^* = 1}$). For or $\boldsymbol{\varphi = 0°}$ or $\boldsymbol{\varphi = 90°}$, the perturbation function $\boldsymbol{\psi_1}$ has a symmetric bicellular model of the fluid in the vertical while perturbation function of second order $\boldsymbol{\psi_2}$ gives four identical cells and symmetrical relative to the center of the cavity. The isothermal $\boldsymbol{T_1}$ are anti-symmetrical about the mid-height of the cavity $(\boldsymbol{x = A/2})$.

The temperature field $\boldsymbol{T_2}$ shows a remarkable change when $\boldsymbol{\varphi}$ goes from $\boldsymbol{0°}$ to $\boldsymbol{90°}$. The maximum values of perturbation functions $(\boldsymbol{\psi_1}, \boldsymbol{\psi_2})$ decrease as the value of the angle of orientation of anisotropy increases. Fig. 6 ($\boldsymbol{\varphi = 0°}$, $\boldsymbol{K^* < 1}$) and Fig. 8 ($\boldsymbol{\varphi = 90°}$, $\boldsymbol{K^* > 1}$) illustrate perturbation functions who are similar to those shown respectively in Fig. 7 ($\boldsymbol{\varphi = 90°}$, $\boldsymbol{K^* > 1}$) and Fig. 5 ($\boldsymbol{\varphi = 0°}$, $\boldsymbol{K^* < 1}$).

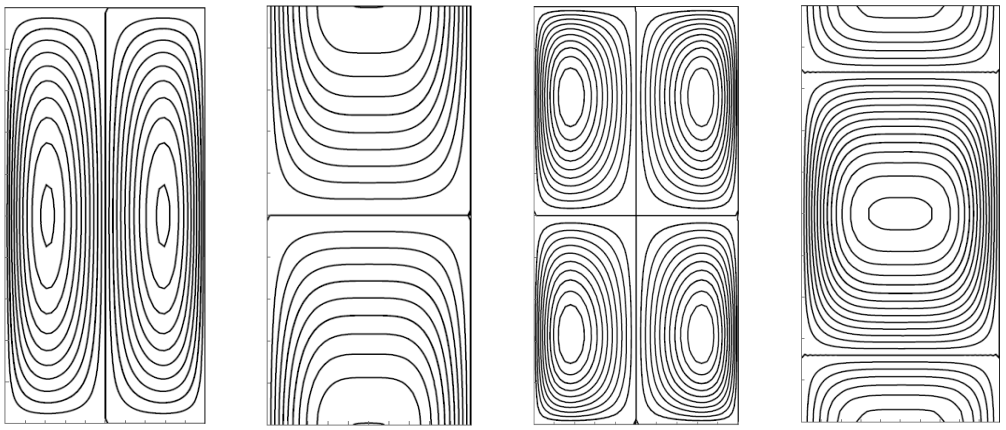

Fig. 5. Streamlines and isotherms for $\boldsymbol{k^* = 1, K^* = 100}$ and $\boldsymbol{\varphi = 0°}$: a) $\boldsymbol{|\psi_{1_{max}}| = 1.4 \times 10^{-3}}$; b) $\boldsymbol{T_{1_{min}} = -3.31 \times 10^{-5}}$, $\boldsymbol{T_{1_{max}} = 3.31 \times 10^{-5}}$; c) $\boldsymbol{|\psi_{2_{max}}| = 7.04 \times 10^{-8}}$; d) $\boldsymbol{T_{2_{min}} = -1.05 \times 10^{-8}}$, $\boldsymbol{T_{2_{max}} = 4.50 \times 10^{-9}}$

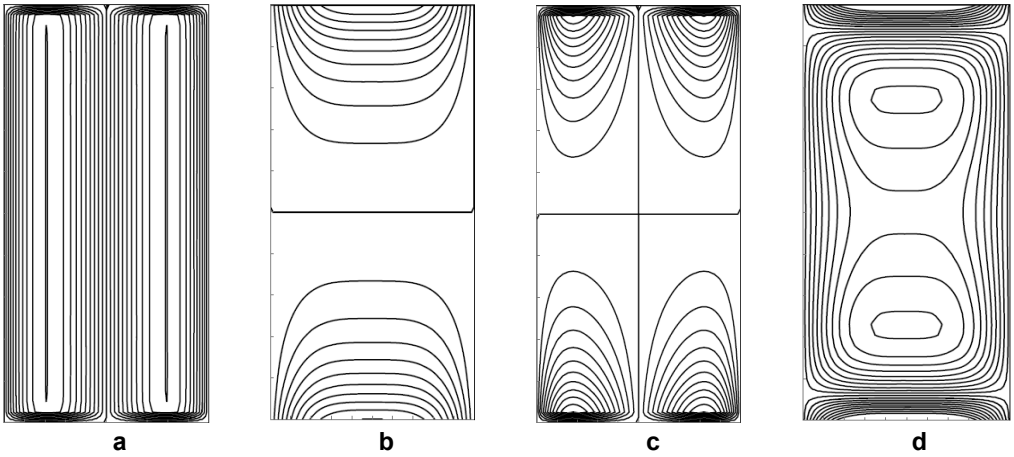

Fig. 6. Streamlines and isotherms for $\boldsymbol{k^* = 1, K^* = 0.01}$ and $\boldsymbol{\varphi = 0°}$: a) $\boldsymbol{|\psi_{1_{max}}| = 8 \times 10^{-3}}$; b) $\boldsymbol{T_{1_{min}} = -4.15 \times 10^{-4}}$, $\boldsymbol{T_{1_{max}} = 4.15 \times 10^{-4}}$; c) $\boldsymbol{|\psi_{2_{max}}| = 2.14 \times 10^{-5}}$; d) $\boldsymbol{T_{2_{min}} = -5.55 \times 10^{-7}}$, $\boldsymbol{T_{2_{max}} = 4.97 \times 10^{-7}}$

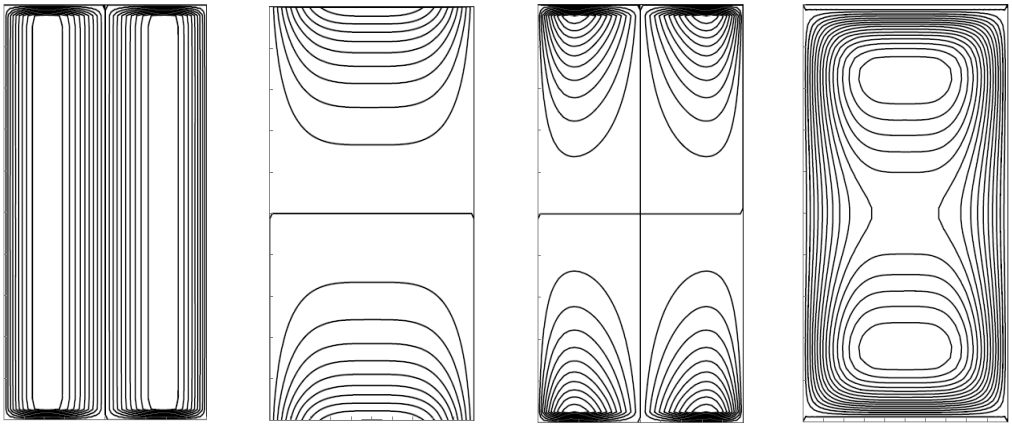

Fig. 7. Streamlines and isotherms for $k^* = 1, K^* = 100$ and $\varphi = 90°$: a) $|\psi_{1_{max}}| = 8.19 \times 10^{-5}$; b) $T_{1_{min}} = -4.15 \times 10^{-6}$; $T_{1_{max}} = 4.15 \times 10^{-6}$; c) $|\psi_{2_{max}}| = 2.14 \times 10^{-11}$; d) $T_{2_{min}} = -5.45 \times 10^{-11}$; $T_{2_{max}} = 6 \times 10^{-12}$

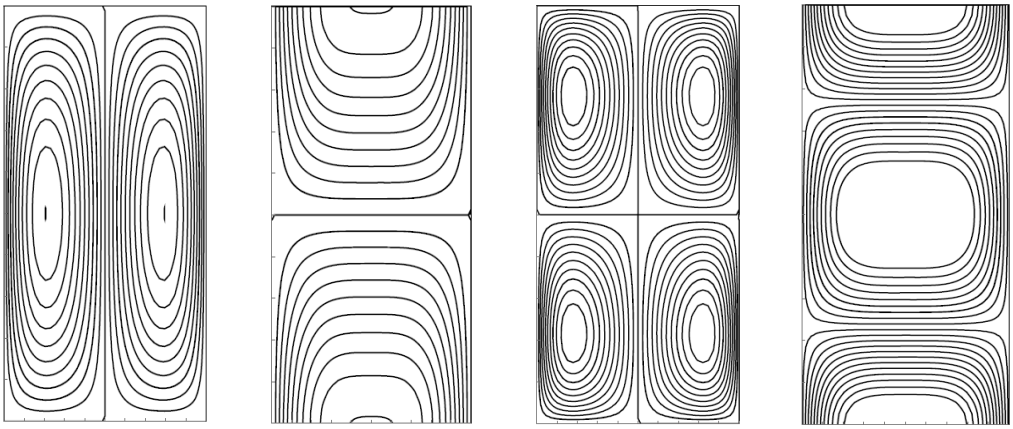

Fig. 8. Streamlines and isotherms for $k^* = 1, K^* = 0.01$ and $\varphi = 90°$: a) $|\psi_{1_{max}}| = 1.43 \times 10^{-1}$; b) $T_{1_{min}} = -3.3 \times 10^{-3}$, $T_{1_{max}} = 3.3 \times 10^{-3}$ c) $|\psi_{2_{max}}| = 7.04 \times 10^{-2}$; d) $T_{2_{min}} = -1.15 \times 10^{-2}$; $T_{2_{max}} = 1.8 \times 10^{-3}$

Figs. 9 and 10 show the isotherms (T_1 and T_2) and the streamlines of (ψ_1 and ψ_2) when the anisotropy ratio permeability and the angle of orientation of anisotropy are kept constant ($K^* = 1$, $\varphi = 0°$) and the thermal conductivity anisotropy ratio varies from 0.01 to 100. The structure of the heat flux generated by ψ_1, does not change when k^* varies. This result is consistent with our expectations for that the expression of ψ_1 which is independent of the conductivity anisotropy ratio (Eq. 30).

When $k^* = 0.01$, the elements of ψ_2, T_1 and T_2 **';[po**disappear in the central region of the cavity and present only flattened cells to the upper and lower walls ($x = 0$ and $x = A$) of the cavity. For $k^* = 100$, the heat flux inside the cavity develops in the form of thermal boundary layer along the vertical cold wall. Except the perturbation function ψ_1, the reduction in the anisotropy ratio of thermal conductivity contributes to an increase in the maxima of the other perturbations functions.

The effects of the orientation angle φ relating to the main axes of permeability of the porous medium on the average rate of heat transfer are shown in Fig. 11. There is a symmetry results with respect to $\varphi = 90°$ and this remark leads us to limit the discussion to the field angle φ such

as $0 < \varphi < 90°$. Thus, the figure reveals that when the anisotropic permeability ratio is less than unity ($K_1 < K_2$), the Nusselt number is maximum when the angle of orientation $\varphi = 0°$ (Maximum permeability in the vertical direction) and minimum when $\varphi = 90°$ (A minimum permeability in the vertical direction). The opposite is true when the anisotropy ratio permeability is greater than unity ($K^* > 1$). Heat transfer by convection is minimal when the orientation angle $\varphi = 0°$ and maximum when $\varphi = 90°$.

Fig. 12 shows the effects of Rayleigh number on the Nusselt number for different values φ of the orientation angle φ for anisotropy ratios conductivity and permeability respectively $k^* = 1$ and $K^* = 10$ with the aspect ratio $A = 2$. We notice in this Fig. 12, an increasing rate of the heat transfer when the orientation angle φ increases from 0 to $90°$. Similarly, one can easily observe that the heat transfer rate decreases rapidly with increasing Rayleigh number that characterizes the effects of buoyancy force. This behavior is explained by the presence of a source of heat within the cavity, which forces the fluid more heat inside, to move the colder side walls. During this movement the fluid temperature decreases.

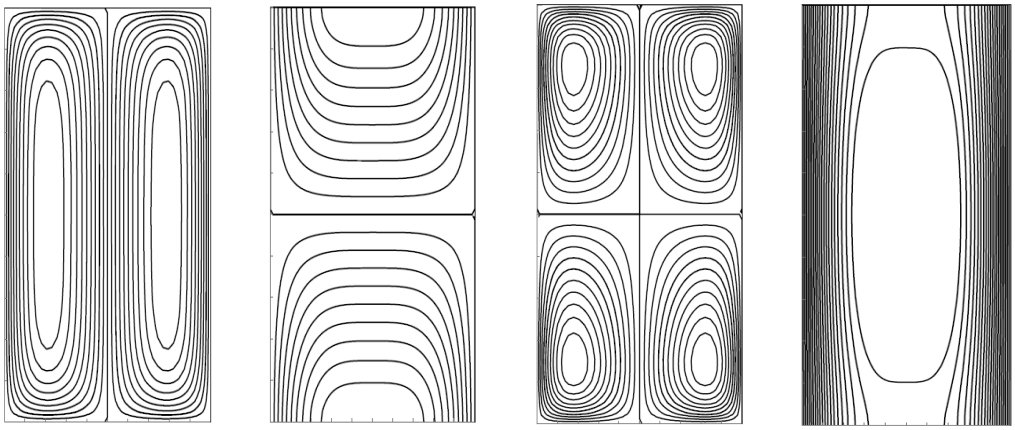

Fig. 9. Streamlines and isotherms for $k^* = 100, K^* = 1$ and $\varphi = 0°$: a) $|\psi_{1_{max}}| = 8 \times 10^{-3}$; b) $T_{1_{min}} = -1.20 \times 10^{-7}$, $T_{1_{max}} = 1.20 \times 10^{-7}$; c) $|\psi_{2_{max}}| = 4.68 \times 10^{-9}$; d) $T_{2_{min}} = -8.25 \times 10^{-11}$, $T_{2_{max}} = 0$

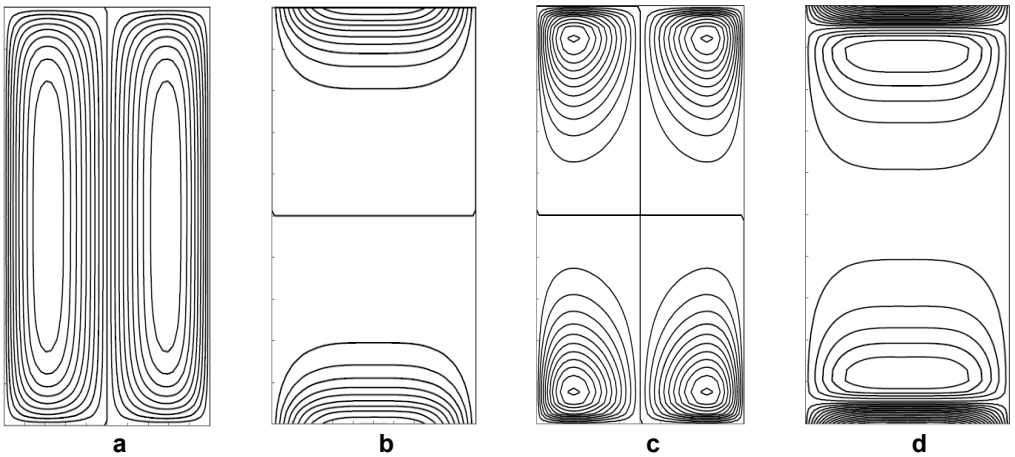

Fig. 10. Streamlines and isotherms for $k^* = 0.01, K^* = 1$ and $\varphi = 0°$: a) $|\psi_{1_{max}}| = 8 \times 10^{-3}$; b) $T_{1_{min}} = -7.07 \times 10^{-2}$; $T_{1_{max}} = 7.07 \times 10^{-2}$; c) $|\psi_{2_{max}}| = 10^{-3}$; d) $T_{2_{min}} = -1.64 \times 10^{-3}$, $T_{2_{max}} = 4.37 \times 10^{-4}$

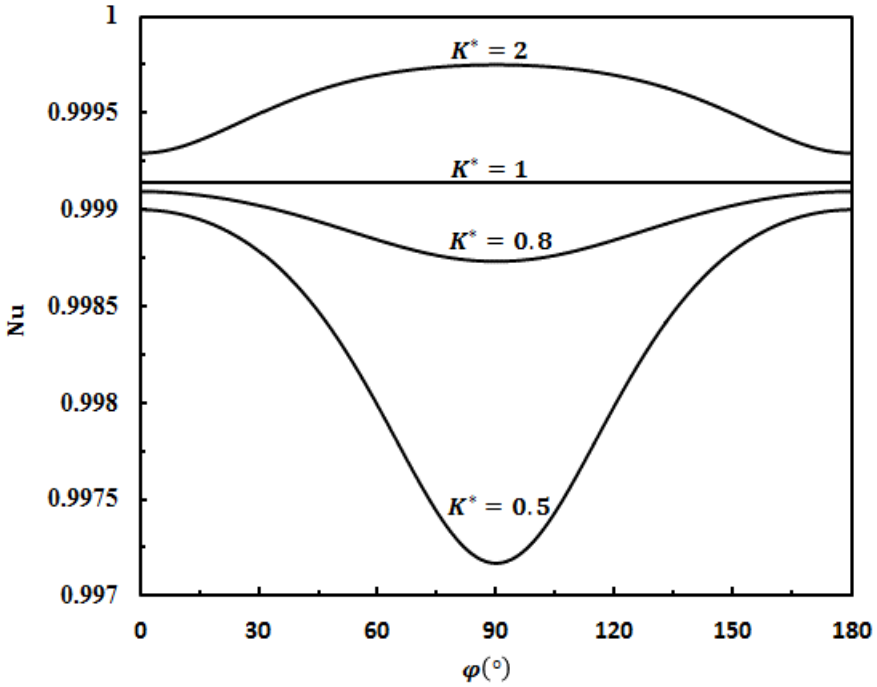

Fig. 11. Effects of the inclination angle φ and anisotropic permeability ratio K^*on Nusselt number, for $k^* = 1, A = 2$ and $Ra = 20$

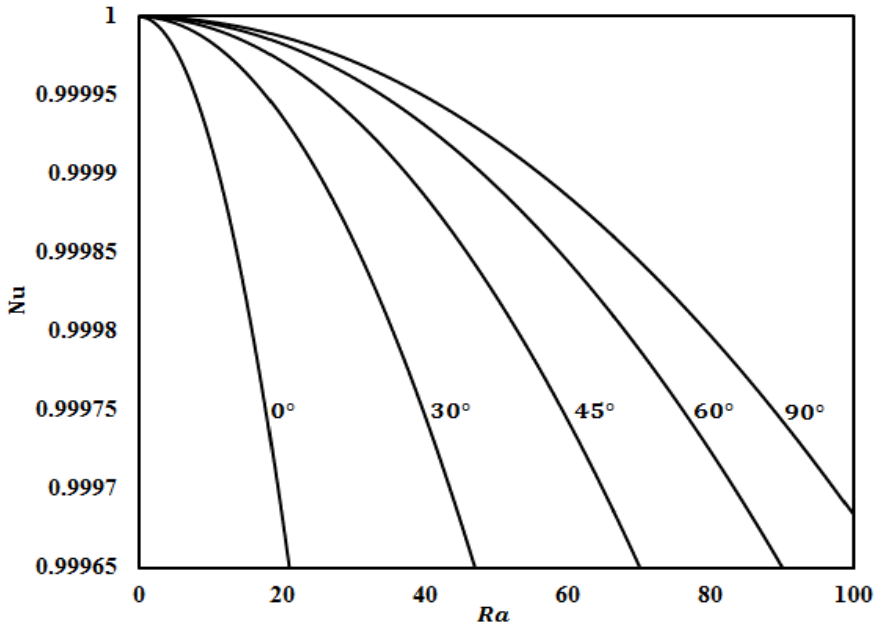

Fig. 12. Nusselt number variation as a function of Ra for different values of orientation angle φ $(k^* = 1, K^* = 10$ and $A = 2)$

Figs. 13 and 14 illustrate the variation of the heat transfer rate of fluid as a function of anisotropy ratio with respect to permeability K^* and conductivity k^*. The curves show that the heat transfer by convection increases with an increase of anisotropy ratio and tend asymptotically

toward unity. It is noticed that, for a given value of the anisotropy ratio, the Nusselt number increases with a decrease of the Rayleigh number.

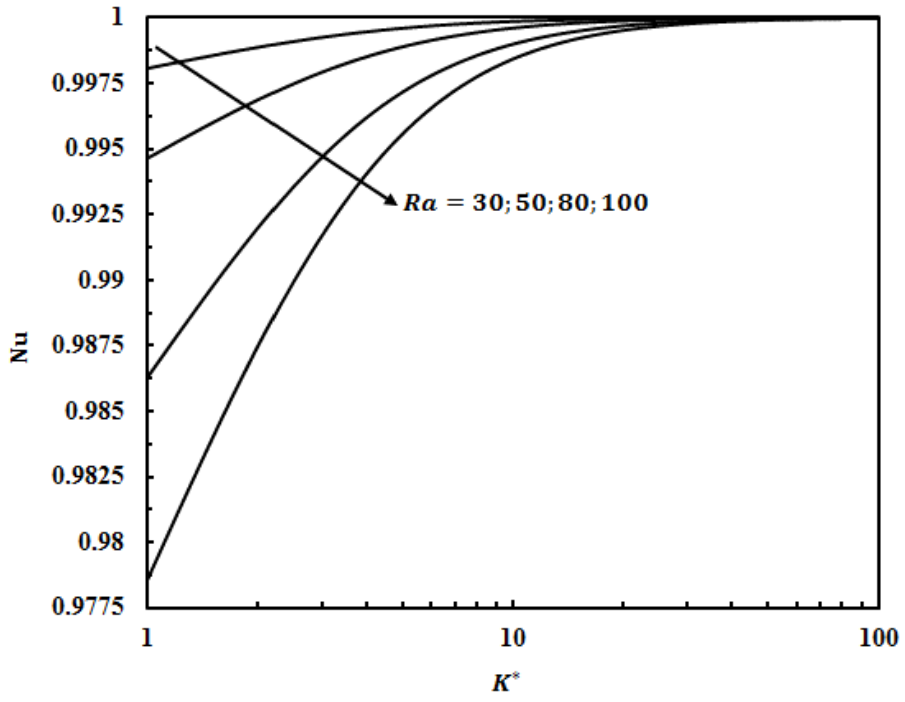

Fig. 13. Nusselt number variation as a function of K^* for different values of Rayleigh number Ra ($k^* = 1, \varphi = 30°$ and $A = 2$)

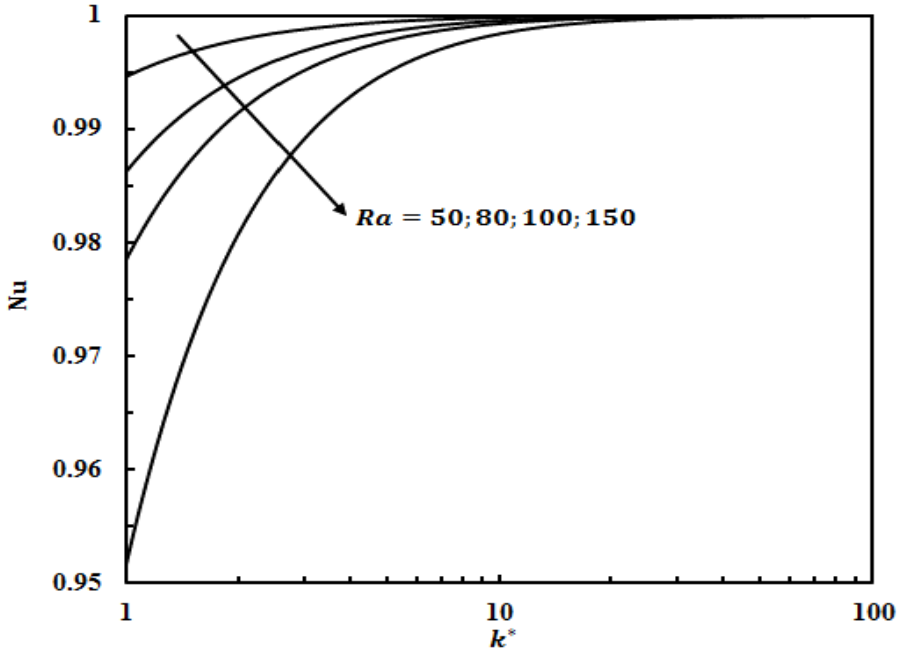

Fig. 14. Nusselt number variation as a function of k^* for different values of Rayleigh number Ra ($K^* = 1, \varphi = 30°$ and $A = 2$)

5. CONCLUSION

We have studied the effects of anisotropy parameters in permeability and thermal conductivity of the heat transfer, in a vertical cavity filled with a porous medium saturated by a Newtonian fluid. The perturbation method is used to determine the streamlines, isotherms and heat transfer rate. Analyzing the results obtained, it emerges the following conclusions:

- The distribution of the streamlines and the temperature fields in the vertical cavity are greatly influenced by the permeability anisotropy parameters ($\boldsymbol{K^*, \varphi}$) and thermal conductivity $\boldsymbol{k^*}$.
- The heat transfer in the cavity is minimum (maximum) when the main axis having the high permeability which is oriented parallel (perpendicular) to the gravity vector.
- When increasing the Rayleigh number, the convective flow in the vertical cavity containing the heat source decreases.

COMPETING INTERESTS

Authors have declared that no competing interests exist.

REFERENCES

1. Meffert H. F. Th., Potters ML. Development of the temperature field in a cube with heat generation. Ann. Bull IIR. 1970;1: 97–106.
2. Rooda Eelkman J, Van Beckum FPH. Heat transfer during the cooling process of exponential heat generating produce, Lebensm. Wiss. Technol. 1978;2:209–214.
3. Hwang IT. Finite amplitude thermal convection in porous media with heat source and variable viscosity PhD thesis, University of Minnesota; 1971.
4. Buretta R. Thermal convection in a fluid filled porous layer with uniform internal heat source PhD dissertation, University of Minnesota; 1972.
5. Sun WJ. Convective instability in superposed porous and free layers. PhD Thesis, University of Minnesota; 1973.
6. Gabor JD, Sowa ES, Baker L, Cassulo JC. Studies and experiments on heat removal from fuel debris in sodium. Proc. Fast Reactor Safety Mtg., Beverly Hills, California, April 2 – 4, Conf. – 740401 – P2:823 – 844 U.S. atomic energy commission; 1974.
7. Gasser RD, Kazimi MS. Onset of convection in a porous medium with internal heat generation. J. Heat Transfer. 1976;98:49–54.
8. Hardee HC, Nilson RH. Natural convection in porous media with heat generation. Nuclear Science and Engineering. 1977; 63:119–132.
9. Bergholz RF. Natural convection of a heat generation fluid in a closed cavity. J. Heat Transfer. 1980;102:242–247.
10. Gill AE. The boundary-layer Regime for convection in a rectangular cavity. J. Fluid Mech. 1966;25:515–536.
11. Emara AA, Kulacki FA. A numerical investigation of thermal convection in a heat-generating fluid layer. ASME Paper No. 79 – HT – 103.
12. Beukema KJ, Bruin S, Schenk J. Three-dimensional natural convection in a confined porous medium with internal heat generation. Int. J. Heat Mass Transfer. 1983;26(3):451–458.
13. Haajizadeh M, Ozguc AF, Tien CL. Natural convection in a vertical porous enclosure with internal heat generation Int. J. Heat Mass Transfer. 1984;27(10):1893–1902.
14. Acharya S, Goldstein RJ. Natural convection in an externally heated vertical or inclined square box containing internal energy source. ASME J. Heat Transfer. 1985;107:855–866.
15. Prasad V. Thermal convection in a regular cavity filled with a heat generation, Darcy porous medium. J. Heat Transfer. 1987; 109:697-703.
16. Churbanov AG, Vabishchevich PN, Chudanov VV, Strizhov VF. A numerical study on natural convection of a heat generating fluid in rectangular enclosure. Int. J. Heat Mass Transfer. 1994;37(18): 2969–2984.
17. Kim Gi Bin, Hyun Jae Min. Buoyant convection of a power law fluid in an enclosure filled with heat generating porous media. Numerical Heat Transfer, Part A. 2004;45:569–582.
18. Degan G, Vasseur P. Natural convection in a vertical slot filled with an anisotropic porous medium with oblique principal

axes. Numerical Heat Transfer, Part A. 1996;30:397–412.
19. Bear J. Dynamic of fluid in porous media. American Elsevier Publishing Company, New York; 1972.
20. Kantorovich LV, Krylov VI. Approximate methods of higher analysis. Noordhoff, the Netherlands. 1958;304–327.

Peer-review history:
The peer review history for this paper can be accessed here:
http://www.sdiarticle4.com/review-history/61707